

WIND CHAPTER

PERCY LINK

1. INTRODUCTION

The previous chapter illustrated that changes in land surface heat fluxes, as mediated by plant stomatal dynamics, can change atmospheric boundary layer temperature and evaporative demand in California. In this chapter, we investigate the effect of changes in land surface heat fluxes, controlled by modified soil moisture, on near-surface winds in California. We focus on winds at a specific wind farm, the Solano Wind Project in the Sacramento-San Joaquin River Delta region of California. A regional atmospheric model is used to test the sensitivity of Solano winds to different regions' soil moisture and to quantify the magnitude of the effect at different times of day across a range of soil moisture changes. This study serves as a prototype for characterizing the importance of soil moisture information for wind forecasts at other wind farms. We aim to demonstrate that accurate soil moisture information can improve wind forecasts.

Accurate wind forecasts can reduce the cost of integrating wind energy into the electric grid on a large scale. In order to reduce CO₂ emissions to the degree necessary to avert dangerous climate change [IPCC, 2013], electric utilities will need to transition to non-fossil-fuel energy sources, including a large fraction of wind energy [Jacobson and Delucchi, 2011]. However, although wind energy has large peak generation potential, it is intermittent, and the instantaneous mismatch between wind generation and electric demand must be met with other generation.

Date: 23:23 Thursday 16th October, 2014.

In most utilities, allocations of conventional electric generation (coal, natural gas, hydroelectric, and nuclear) are made a day ahead, based on forecasted net demand (demand minus wind and solar supply). At shorter lead times (hour-ahead to real-time), imbalances between the day-ahead allocations of conventional generation and the actual net demand must be met with, in the case of a shortfall, more expensive quick-startup generation, or in the case of excess generation, wasted energy resources. These imbalance costs add significantly to the cost of wind energy (around 10% of a wind generator's income in a liberalized market [Fabbri *et al.*, 2005]). Improved accuracy of wind forecasts could reduce imbalance costs, making integration of wind into the electric grid more economically feasible: wind and solar forecasting could reduce energy costs by \$0.01 to \$0.02 per kWh at 30% wind and solar penetration [GE Energy, 2010], or 8-15% of the average US cost of electricity (\$0.13/kWh in July 2014 [EIA, 2014]); and at high wind penetration, \$68 million to \$160 million could be saved annually in California using current state of the art forecasting, with an opportunity to save \$19 million to \$38 million more with forecast accuracy improvements [Porter and Rogers, 2010].

The major wind forecasting companies in North America and Europe use numerical weather prediction (NWP) models to make their day-ahead forecasts, often in combination with statistical post-processing [Porter and Rogers, 2010; Foley *et al.*, 2012; Monteiro *et al.*, 2009]. NWP models simulate atmospheric wind speed, temperature, pressure, and humidity (among other variables) by solving the equations for conservation of momentum, mass, and energy, discretized in three spatial dimensions and in time. Regional NWP models require boundary condition information at the lateral boundaries of the grid, as well as bottom boundary fluxes of energy, moisture, and momentum. If the bottom boundary is land, these fluxes are usually calculated with a land surface model. Wind energy forecasts are sensitive

to NWP model resolution and physical parameterizations, especially planetary boundary layer (PBL) schemes [Draxl *et al.*, 2014; Marjanovic *et al.*, 2014]; the optimal PBL scheme depends in part on atmospheric stability conditions [Draxl *et al.*, 2014; Marjanovic *et al.*, 2014], and the optimal grid resolution depends largely on terrain complexity, with more complex terrain requiring higher resolution [Marjanovic *et al.*, 2014, Carvalho *et al.*, 2012]. Ensembles of NWP runs have been used to characterize a forecast probability distribution [Deppe *et al.*, 2013; Pinson and Madsen, 2009]. Various model output statistics (MOS) algorithms incorporating historical observations have been shown to improve NWP forecasts in post-processing; in particular, machine learning algorithms such as directional multipoint linear regression [Bédard *et al.*, 2013], multiple linear regression [Ranaboldo *et al.*, 2013], random forests, generalized linear models, gradient boosting, and support vector machines [Ellis *et al.*, 2014; Ortiz-García *et al.*, 2011], and neural networks [Kusiak *et al.*, 2009] have shown promise. The prediction of ramps (rapid increases or decreases in wind power) remains a challenge [Carcangiu *et al.*, 2014; Ellis *et al.*, 2014; Wharton *et al.*, 2011].

Fluxes of energy at the land surface are known to influence regional circulations, yet the influence of soil moisture and land surface heating on wind prediction has received little attention in the wind energy forecasting literature. Soil moisture heterogeneity, and the resulting contrasts in sensible heat flux, can drive mesoscale circulations on land with wind speeds of several m/s [Chen and Avissar, 1994; Avissar and Schmidt, 1998]. Thermal contrast between land and ocean can drive sea-breeze circulations with wind speeds up to 10 m/s [Miller *et al.*, 2003], and the strength of the thermal contrast and of the resulting wind depends in part on soil moisture because of its influence on land surface temperature [Physick, 1980]. In one of the few wind energy papers to discuss the effect of soil moisture on wind

forecasts, Marjanovic *et al.* [2014] show that the forecast at a California wind farm is sensitive to initial soil moisture, and in a related study, Wharton *et al.* [2011] show that soil moisture can be important for forecasting wind ramps.

Winds at the Solano wind farm are likely to depend on soil moisture because they are strongly influenced by the contrast of land surface heating with the adjacent cool ocean [Zhong *et al.*, 2004]. Solano sits in a valley pass between the ocean and California's Central Valley, and onshore winds are channeled and accelerated through the pass; this topographic channeling also constrains the wind direction at low levels near Solano to remain near westerly [Zhong *et al.*, 2004; Mansbach, 2010]. The diurnal cycle of land surface heating drives a marked diurnal cycle in wind speed in the Solano area, with minimum wind speeds in the morning and maximum speeds in the late afternoon and evening [Zhong *et al.*, 2004; Mansbach, 2010]. Additionally, the strongest winds occur in the summer at Solano, in part due to generally calm synoptic conditions (created by the north Pacific summertime high pressure) that allow the strong surface temperature contrast between ocean and land to drive onshore flow [Zhong *et al.*, 2004; Mansbach, 2010]. Because winds at Solano are generated partly by land surface heating contrasts, it is likely that errors in soil moisture initial conditions would create errors in NWP wind forecasts.

Better soil moisture information may improve wind forecasts at Solano and similar sites. As such, we seek to understand the sensitivity of Solano wind to soil moisture, and the physical mechanism underlying the sensitivity. **Say something about how the model is an imperfect representation of the world; it captures many of the important processes, but we do not contend that it represents land surface fluxes perfectly. In this study, we are investigating both the real-world physical sensitivity of the winds to soil moisture,**

to the degree possible given the model errors; and also characterizing the sensitivity within the model, even if that sensitivity is not fully realistic, because this tool is in common usage in wind energy forecasting, and thus it is important to understand the sensitivity of the tool to the inputs. We investigate the following questions:

- On which regions' soil moisture do Solano winds depend?
- At what time of day is Solano wind most sensitive to soil moisture? What changes in the amplitude and timing of the wind diurnal cycle result from changes in soil moisture?
- How do wind forecast errors scale with soil moisture changes/errors? Are there particular ranges of soil moisture where wind forecasts are particularly sensitive?
- What is the physical mechanism for soil moisture's influence on Solano winds?

To answer these questions, we conduct experiments with a regional atmospheric model commonly used in wind energy forecasting research. We perturb soil moisture in different California regions and to different degrees and quantify the response of Solano turbine-level wind magnitude and timing. Moreover, we identify regional pressure changes that correlate with wind changes and relate them to changes in surface heating; and we attribute changes in wind to changes in the terms of the momentum budget.

2. METHODS

The sensitivity of Solano wind forecasts to soil moisture is tested using experiments with a regional atmospheric model, the Weather Research and Forecasting (WRF) model. The WRF model, described in detail in Skamarock et al. [2008], is

Domain	Δx (km)	Δy (km)	n_x	n_y	n_z	Δt (s)	USGS data res
d01	8.1	8.1	96	99	45	45	2 min
d02	2.7	2.7	175	175	45	15	2 min

TABLE 1. Model domains

a three-dimensional, non-hydrostatic regional atmospheric model with σ vertical coordinates that follow the terrain near the surface and transition to horizontal at high altitude. WRF solves the discretized equations for conservation of momentum, mass, energy, and scalars like water vapor, and it has a range of parameterization options for radiation, planetary boundary layer (PBL) turbulence, cloud microphysics, convection, bottom boundary fluxes of water vapor and heat, and lateral boundary forcing. WRF has been used extensively in wind energy forecasting [CITATIONS], with generally good performance [CITATIONS]. Accuracy of WRF-forecasted turbine-level winds depends on (*resolution, PBL scheme, lateral forcing, soil moisture* ***) [CITATIONS].

2.1. Model setup. We run WRF with two two-way-nested domains centered on the Solano wind farm (Figure 1); the domains are described in Table 1. The finest resolution presented here is 2.7 km; preliminary tests with a third finer grid (0.9 km) showed little change in the forecasted winds, similar to the results of Marjanovic et al. [2014], who found little accuracy improvement with horizontal resolution below 2.7 km in their simple terrain case. The domain has 45 vertical levels, with a minimum spacing of **XX** near the surface and a maximum spacing of **XX** at the top of the model domain; turbine-level (60-100 m) wind forecasts are not very sensitive to vertical resolution beyond about 40 levels [Marjanovic et al., 2014, and references therein].

The atmospheric model is coupled to the Noah land surface model with USGS land use and soil classifications. The observed distribution of land use and soil

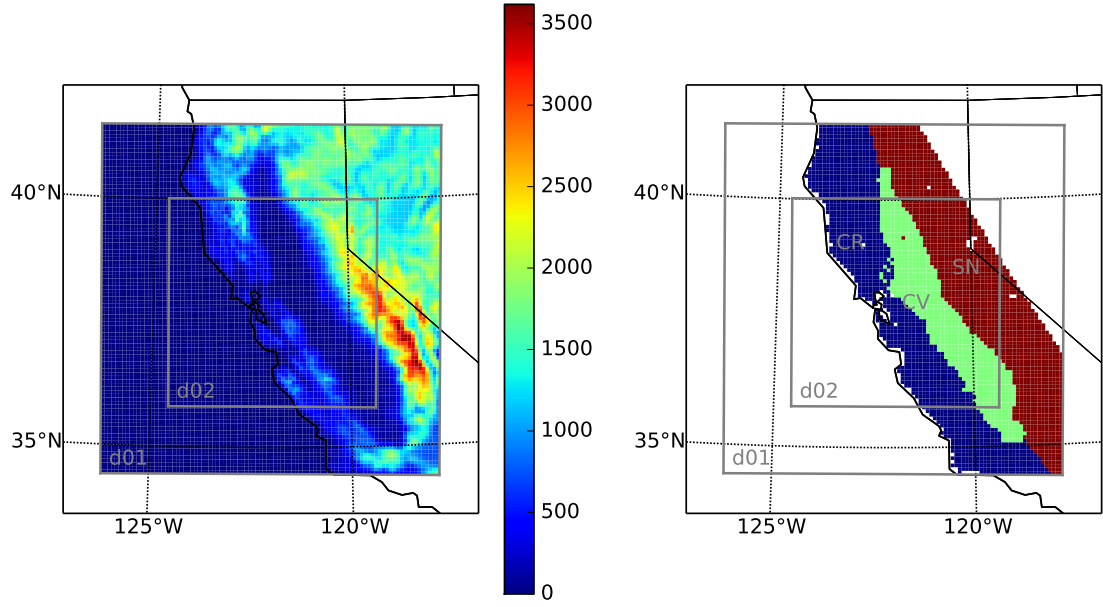


FIGURE 1. WRF model domains, showing (a) topographic height in m, and (b) the Coast Range (CR), Central Valley (CV), and Sierra Nevada (SN) regions for soil moisture tests.

types are used, as are the default vegetation water-use parameters for each land use type, in order to simulate as closely as possible the real present day sensitivity of Solano winds to soil moisture. Uncertainties associated with errors in the model representation of water movement in the subsurface and plant water use are addressed in the Discussion.

The ACM2 PBL scheme is used, following the recommendations of Marjanovic et al. [2014] for a locally forced simple terrain case in California; this PBL scheme includes both local (small-scale turbulent) and nonlocal (large convective plume) vertical transport, and can thus simulate both stable and unstable conditions [Pleim, 2007]. The model is forced at the lateral boundaries with AWIP reanalysis at **XX km** resolution [**CITATION**]. Other parameterization schemes and settings are listed in Table 2. Model variables are output every 30 minutes.

Scheme	Setting
WRF version	3.6
Grid nesting	two-way
Lateral boundary conditions	AWIP
Soil levels	4
Land use and soil categories	USGS
Land surface model	Noah
Surface layer	MM5 Monin-Obukhov
Planetary Boundary Layer (PBL)	ACM2
Microphysics	WSM 3-class simple ice
Longwave radiation	RRTM
Shortwave radiation	Dudhia
Cumulus	Kain-Fritsch (new Eta)
Turbulence closure	Horizontal Smagorinsky first order
Momentum advection	5th order horizontal, 3rd order vertical
Scalar advection	Positive definite
Lateral boundary	5 grid points

TABLE 2. WRF parameterization options. See **ARW USERS' GUIDE** for description of schemes.

All experiments are run for the period 2009-06-26 00:00 UTC to 2009-07-11 00:00 UTC, and the first **32** hours are discarded as model spin-up. This period was chosen for several reasons: (1) it contains a range of synoptic conditions (weak background wind June **27-July 5**, and strong background wind July **6-10**), (2) turbine-level wind speeds in this region are highest in the spring and summer [**WIND CLIMATOLOGY THESIS, WHARTON**], and (3) the sensitivity to soil moisture is expected to be strongest in the warm season, because radiation incident to the land surface is greatest in the warm season, so changes in the relative partitioning between evapotranspiration and sensible heat flux have the largest absolute magnitude then.

2.2. Soil moisture experiments. The model experiments are listed in Table 3. In the first set of experiments, we test the sensitivity of Solano winds to soil moisture in different large-scale regions of California. In cases dryCR, dryCV,

and drySN, the background volumetric soil moisture (model variable SMOIS, m^3 water/ m^3 total volume) is set to 0.25, and the soil moisture of the test region (respectively, the Coast Range, Central Valley, and Sierra Nevada, shown in Figure 1b) is set to 0.1. In cases wetCR, wetCV, and wetSN, the background soil moisture is set to 0.1, and the soil moisture of the test region is set to 0.25.

The next set of experiments tests how the Solano wind response scales with soil moisture in the Central Valley, in both a normal-to-wet background (mountain) scenario and a dry background scenario. In cases CVXX (where XX is a numeric value), the Coast Range and Sierra Nevada regions' soil moisture is set to 0.2, and the Central Valley soil moisture is set to the value specified by XX. In cases CVXXdry, the Coast Range and Sierra Nevada regions' soil moisture is set to 0.1, and the Central Valley soil moisture again is specified by XX.

In all cases, the soil moisture is set to the prescribed values at the model start time (2009-06-26 00:00 UTC) and is reset to the prescribed value each day at 08:00 UTC (midnight Pacific Standard Time); the soil moisture evolves according to the land surface model each day between resets. The change in soil moisture between resets is **small** (**Figure XX**).

2.3. Model output analysis.

2.3.1. *Wind – pressure-anomaly regression maps.* The relationship between pressure spatial patterns and Solano turbine-level wind is quantified using linear regression. At each output time t , the pressure anomaly at grid point (i, j) and vertical level k is calculated as

$$(1) \quad p'_{i,j,k,t} = p_{i,j,k,t} - \overline{p_{k,t}},$$

Run name	Background SMOIS	Perturbed SMOIS region	Perturbed SMOIS value
CA-0.1	0.1	none	n/a
CA-0.2	0.2	none	n/a
CA-0.25	0.25	none	n/a
dryCR	0.25	Coast Range	0.1
dryCV	0.25	Central Valley	0.1
drySN	0.25	Sierra Nevada	0.1
wetCR	0.1	Coast Range	0.25
wetCV	0.1	Central Valley	0.25
wetSN	0.1	Sierra Nevada	0.25
CV0.05	0.2	Central Valley	0.05
CV0.1	0.2	Central Valley	0.1
CV0.15	0.2	Central Valley	0.15
CV0.25	0.2	Central Valley	0.25
CV0.3	0.2	Central Valley	0.3
CV0.35	0.2	Central Valley	0.35
CV0.05dry	0.1	Central Valley	0.05
CV0.15dry	0.1	Central Valley	0.15
CV0.2dry	0.1	Central Valley	0.2
CV0.25dry	0.1	Central Valley	0.25
CV0.3dry	0.1	Central Valley	0.3
CV0.35dry	0.1	Central Valley	0.35

TABLE 3. Model experiments

where $\bar{p}_{k,t}$ is the horizontally averaged pressure at level k and time t . The time series of pressure anomalies at each grid point is linearly regressed against the time series of turbine-height Solano wind, and the regression slopes and correlated coefficients for all grid points at a given level are mapped (e.g., Figure XX). The same procedure is conducted for the difference in pressure anomalies and wind speed between model test runs and control runs (e.g., Figure XX).

3. RESULTS

We first characterize the differences in Solano turbine-level wind resulting from the soil moisture tests (Section 3.1). We then investigate the physical mechanism

linking changes in soil moisture to changes in Solano wind timing and magnitude (Section 3.2).

3.1. Characterization of Solano wind sensitivity to soil moisture.

3.1.1. *Regional sensitivity.* Before presenting the Solano winds, we quantify the synoptic and land-surface-heating forcing in each case, and we characterize the control case winds. The synoptic forcing, measured by wind speed at XX m, varies little between the model runs (Figure XX), and synoptic winds are weak on XX days and strong on XX days. Soil moisture declines by XX m³/m³ or less before being reset each midnight (Figure XX). Land surface heating **DESCRIBE DIFFERENCES HERE**

In both the control and test cases, winds at Solano have a strong diurnal cycle (Figure 2(a)) and tend to be strongest on days with stronger synoptic forcing (July XX). Solano wind speeds are greatest XX to XX hours and are weakest XX to XX hours (Figure 4(a) and Figure 5(a)). Solano winds are strongest in lowest 300 m, particularly in hours XX-XX (Figure 6(a)). The two-week average *u*-component of Solano winds (u_{avg}) is westerly at all heights and times, but at heights 300-1000 m the v_{avg} -component of the winds oscillates between northerly in night and morning to slightly southerly in afternoon and evening; below 300 m, v_{avg} is southerly at all hours.

Regional low-level winds in the control case are consistent with previous studies of California surface winds (Figure 7 first column, **CITATIONS**); flow is strong through the Solano pass and splits into northward and southward branches in the Central Valley. The southward branch is stronger than the northward branch at 06:00 and 14:00, and the northward branch strengthens at 18:00 and 00:00. The

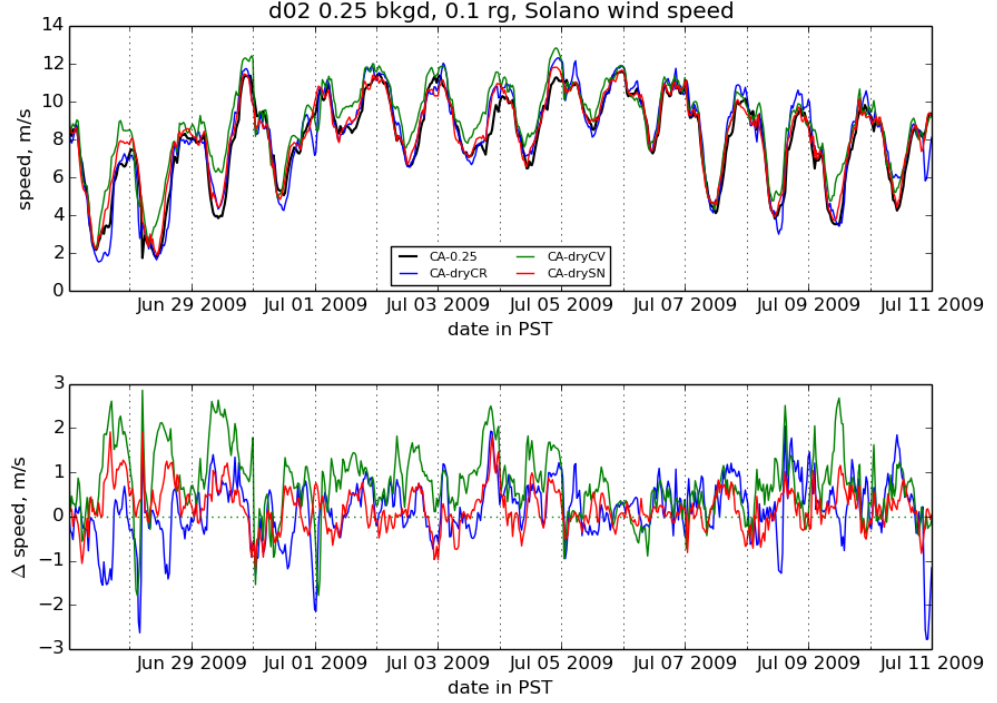


FIGURE 2. Time series of wind speed magnitude at 60 m AGL for the d02 grid point nearest the Solano wind farm, for the wet background and dry perturbation tests. The model spin-up period is excluded.

pressure gradient from the San Francisco Bay to the Central Valley remains strong from 14:00 to 00:00 and weakens by 06:00.

The Solano wind in the regional test cases differs from the control case by as much as 2.5-3 m/s, and the changes are larger on days when the synoptic wind forcing is weaker (Figures 2 and 3, e.g. XX days). The largest changes occur when Central Valley soil moisture is perturbed (dryCR and wetCR).

Drier soils on a wet background increase Solano winds in the afternoon and evening in all regional test cases (Figure 4(b)); the magnitude of this increase is largest in the dryCV case. The increases in both the dryCV and drySN cases are

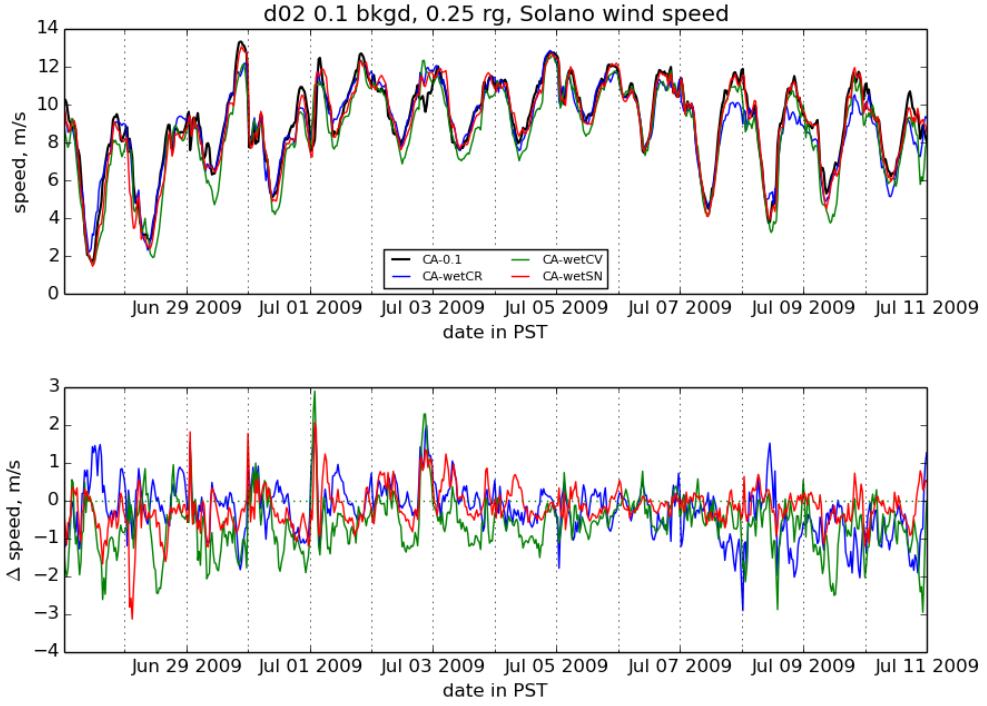


FIGURE 3. Time series of wind speed magnitude at 60 m AGL for the d02 grid point nearest the Solano wind farm, for the dry background and wet perturbation tests. The model spin-up period is excluded.

greatest between 11:00 and 18:00 (1-2 m/s for dryCV and 0.5-1 m/s for drySN), while the increase in the dryCR case happens later, between 16:00 and 21:00 (0.5-1 m/s). Importantly, such increases in the afternoon cause the daily wind speed ramp-up to shift earlier, because the increases occur at the same time as the control ramp-up. Because there are no corresponding decreases at the hour of ramp-down, this means that the duration of the high-wind period also increases. Predicting the timing of ramps is important for utilities, and these results suggest that soil moisture influences ramp-up timing at Solano. Also, drier soils (especially in the Central Valley) increase the minimum wind (XX hours) on many individual days,

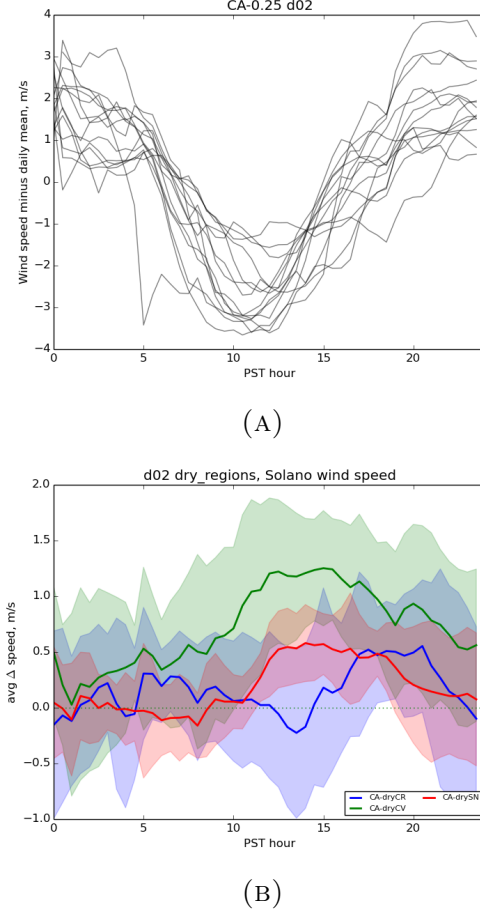


FIGURE 4. (a) Overlaid diurnal cycles of wind speed magnitude minus daily mean wind speed, at 60 m AGL for the d02 grid point nearest the Solano wind farm, for the CA-0.25 control case. (b) Diurnally averaged differences in wind speed, at 60 m AGL for the d02 grid point nearest the Solano wind farm, for the wet background/dry perturbation cases. Shading represents one standard deviation.

especially days with weaker synoptic wind forcing (Figure 2), but these changes do not appear in the two-week average diurnal cycle (Figure 4(b)).

Wetter soils on a dry background have a smaller impact on Solano winds than drier soils on a wet background (Figure 5(b)). Again, the decrease is largest in when Central Valley soil moisture is perturbed. Both the wetCV and wetSN cases have wind decreases during 10:00-18:00 that are more than one standard deviation

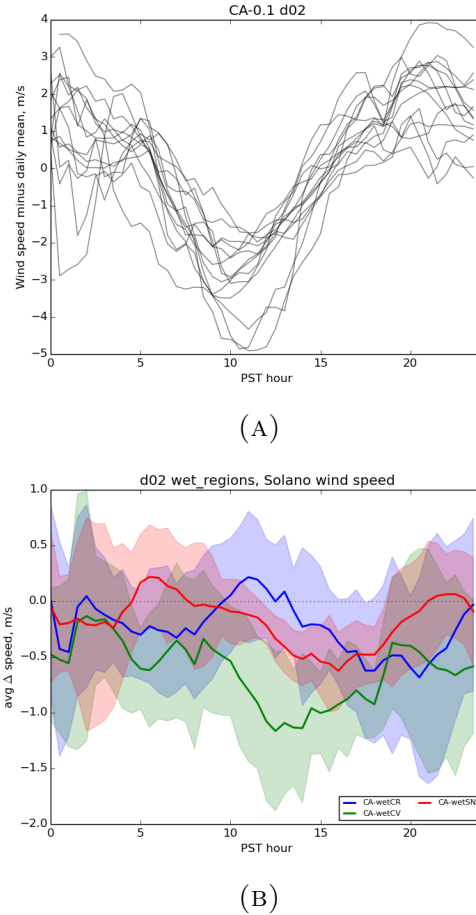


FIGURE 5. (a) Overlaid diurnal cycles of wind speed magnitude minus daily mean wind speed, at 60 m AGL for the d02 grid point nearest the Solano wind farm, for the CA-0.1 control case. (b) Diurnally averaged differences in wind speed, at 60 m AGL for the d02 grid point nearest the Solano wind farm, for the dry background/wet perturbation cases. Shading represents one standard deviation.

from zero (0.25-1.5 m/s for wetCV and 0.2-0.7 m/s for wetSN); for the wetCR case, there are no times of day with wind changes more than one standard deviation from zero.

Vertical profiles: vertical center of increases in each case. Increases in u at all times and at all heights below 1700 m, but differences in magnitude, especially in morning. Changes in v tend to amplify existing diurnal pattern, with more

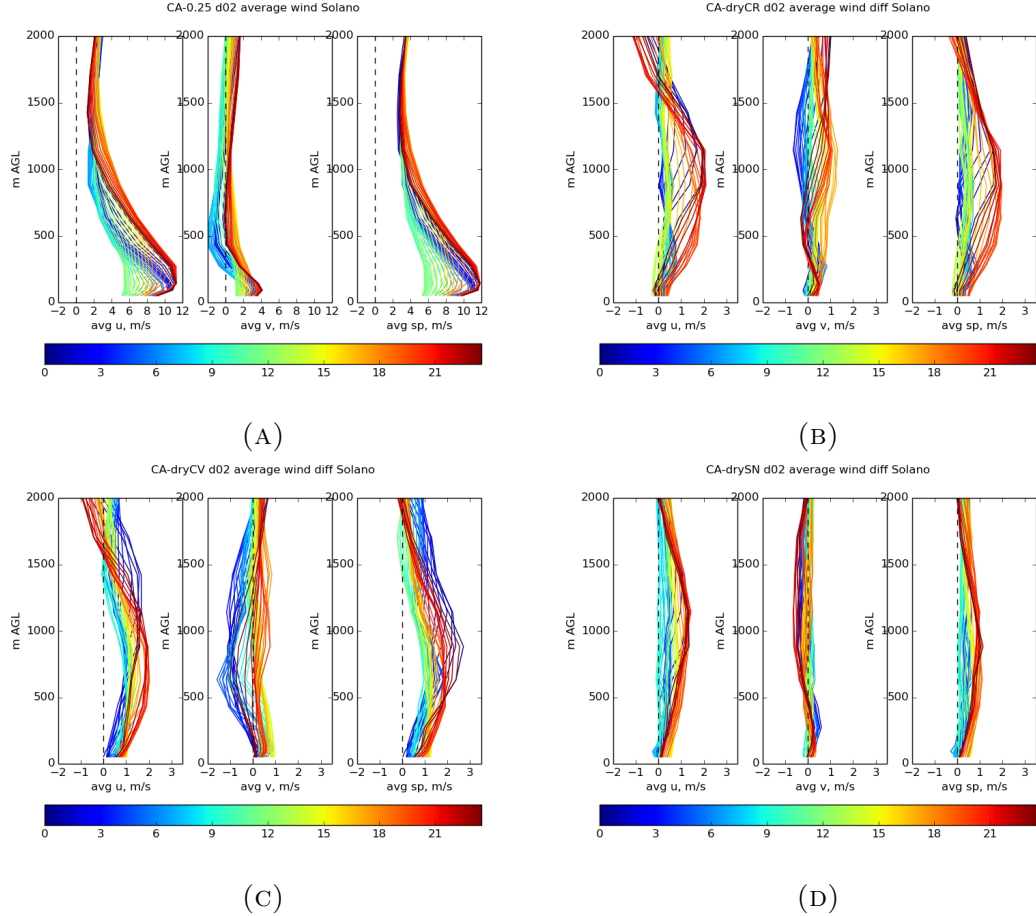


FIGURE 6. Vertical profiles of u , v , and $|u|$, averaged by time of day over the whole simulation (colorbar indicates hour of day in local time), for (a) CA-0.25 control run, and averaged differences from control run for the dry regional test cases: (b) dryCR, (c) dryCV, (d) drySN.

northerly in night and morning and more southerly in afternoon. Degree to which the elevated increases propagate to the ground?

All three test cases show an increase in u at middle levels (500 m - 1000 m). The increase is centered higher in the dryCR and drySN cases (around 1000 m) than in the dryCV case (around 700 m), and the increase extends to the near-surface winds to a greater degree in the dryCV case than in the dryCR or drySN case.

The Solano wind changes occur in the context of larger regional wind and pressure changes (Figure 7). In all dry regional tests, the changes in winds and pressure gradients throughout the Central Valley are largest in the afternoon (second and third rows in Figure 7). In the dry Coast Range test (Figure 7 (e)-(h)), both wind and pressure changes are largest in the northern Central Valley, where cyclonic flow develops around the northern Coast Range. In the dry Central Valley test (Figure 7 (i)-(l)), the pressure gradient from the San Francisco Bay to the Central Valley increases dramatically at 14:00, and these increases persist at 18:00 and to a lesser degree at 00:00. However, at 18:00, the zone of steepest pressure change has been pushed further eastward, and the strongest wind increases track this band of largest pressure gradient. The pattern of wind increases at 00:00 is disorganized, and wind speeds decrease in the southern Central Valley at 06:00. In the dry Sierra Nevada case (Figure 7 (m)-(p)), the pressure gradient strengthens moderately at 14:00 and 18:00, but pressure changes are minimal by 00:00 and 06:00. Wind speeds increase through the Solano pass and the middle Central Valley in the afternoon (14:00 and 18:00), and by 18:00, the bands of largest wind increases have moved outward along Central Valley, again following zones of greatest pressure gradient increase. Wind changes at night (00:00 and 06:00) are small and disorganized.

In summary, the Central Valley soil moisture influences the Solano turbine-level winds more strongly than does the Coast Range or Sierra Nevada soil moisture. Drier soils in all regions, but especially in the Central Valley, increase Solano wind speeds during ramp-up and peak hours (afternoon and evening); drier soils in the Central Valley, especially, shift the daily wind ramp-up earlier. Wetter soils, on the other hand, have a smaller effect on Solano winds; wetter Central Valley soils

cause Solano winds to decrease during ramp-up and peak times (afternoon and evening.)

3.1.2. Scaling of wind changes with Central Valley soil moisture. Drier Central Valley soils increase Solano winds, while wetter Central Valley soils decrease Solano winds (Figure 8.) These changes can be up to 3 m/s, and they occur most consistently in the hours of 12:00 to 22:00 (Figure 9(b)), when they are 0.8-1.7 m/s on average in the driest Central Valley case (CV0.05). The average changes during hours 12:00 to 22:00 scale nonlinearly with CV soil moisture (**shift stats figure**), with larger increases in wind per unit soil moisture decrease when the soil is dry. The greater sensitivity to soil moisture when soils are drier is likely due to the greater sensitivity of surface heating to soil moisture when soils are drier (**forcing figure**), which is related to rapid declines in soil hydraulic conductivity and plant stomatal conductance in the moderate-to-dry soil moisture range (**cite something Bonan? Sap flow paper? Transitional soil moisture regime paper of some kind?**).

3.2. Physical mechanism. Next we investigate the physical mechanism by which changes in soil moisture, especially in the Central Valley, influence near-surface winds at Solano.

The strong diurnal component of the Solano wind (Figures 2 and 3) and the wind speed peak at low levels (Figure 6) suggest significant forcing by land surface heating (consistent with Zhong *et al.* [2004] and Mansbach [2010]). In order to explore the influence of land surface forcing on terms in the momentum budget, we model the topographically channeled wind at Solano as simple one-dimensional flow through the pass governed by a one-dimensional momentum equation,

$$(2) \quad \frac{\partial u}{\partial t} = -u \frac{\partial u}{\partial x} - \frac{1}{\rho} \frac{\partial p}{\partial x} - F\left(\frac{\partial u}{\partial z}, N\right),$$

neglecting Coriolis because of the topographic constraint on wind direction. The first term on the right hand side is the advection of momentum, the second term is the pressure gradient force, and the third term is frictional dissipation as an unspecified function of vertical wind shear and stability (quantified by N , the Brunt-Väisälä frequency). We are interested in the importance of each of these terms through the diurnal cycle and in the influence of soil moisture changes on each of these terms.

3.2.1. *Driving pressure gradient.* In order to identify the pressure gradient most relevant to Solano winds, we linearly regress the horizontal pressure anomaly against Solano turbine-level wind (Section 2.3.1). The regression is repeated for pressure at a range of heights and for a range of lag times, with wind lagging pressure. The regression slopes and correlation coefficients for the control cases (CA-0.25, Figure 10, and CA-0.1, Figure 11) show a consistent pattern of positive slopes and correlation coefficients over the ocean near the central coast (meaning higher pressure in those regions corresponds to faster wind), and negative slopes and correlation coefficients throughout the Central Valley, especially just north and south of the Solano pass (meaning lower pressure in those regions corresponds to faster wind).

Thus, we choose three boxes, shown in gray in Figures 10 to 11, to represent the pressure gradient driving Solano winds. The lag of wind speed behind pressure gradient is evident in the time series of Solano wind and pressure difference between the boxes (Figure 12). Not only does the pressure difference peak 5-6

hours before the Solano wind speed, but the peak pressure difference rapidly dissipates (after 1-2 hours **CHECK THIS**), while the peak wind speed persists for 6-8 hours. Using the pressure difference between the three boxes, we confirm that the peak sensitivity (as measured by the regression slope) and correlation occur with pressure at 110 m ASL (although the metrics are high at all levels below \sim 300 m) with a lag of \sim 4-5 hr for NCV-OCN pressure and \sim 5-6.5 hr for SCV-OCN pressure (Figure 13).

Repeating the regression analysis using test-minus-control changes in pressure and Solano wind, a similar spatial pattern of sensitivity emerges (positive correlation between Solano wind changes and pressure changes in the central coastal ocean, and negative correlation between Solano wind changes and pressure changes in the Central Valley), albeit with weaker correlation (Figures 14 and 15). Again, the changes in wind speed correlate maximally with the changes in pressure at the lowest altitudes (\leq 200 m, Figure 16). In contrast to the control cases which have a 5-6 hour lag, the test-minus-control changes correlate maximally at a lag of \leq 1 hour (Figure 16).

3.2.2. Temperature controls on pressure. The diurnal variations in low-level pressure correspond to diurnal variations in boundary layer temperature, because pressure is the vertical integral of the weight of the air column above a point, and changes in temperature change the density and thus the weight of the air column. Diurnal temperature variations are larger in the Central Valley than over the ocean (Figure 17). In the NCV box, the temperature near the surface (<100 m ASL) declines quickly after sunset, but the temperature aloft in the boundary layer (particularly 300-700 m) remains elevated until at least midnight (Figure 17, panel 2). Both the NCV temperature and the NCV-OCN temperature difference

peak around 17:00. The temperature difference at low levels (<110 m) drops after sunset and approaches zero in the early morning some days, but the temperature difference remains positive at 110-490 m on most days, with NCV warmer than OCN by up to 12 deg C even in the early morning. The near-surface cooling in the Central Valley is due to a combination of radiative cooling of the land surface and advection of cooler marine air by the low-level wind maximum. The pressure difference is most negative (strongest gradient) at the same time as the temperature difference, around 17:00, and is smallest in magnitude (weakest gradient) just before sunrise, around 06:00, when the NCV boundary layer is coolest.

The changes in soil moisture affect the pressure gradient by changing surface heat fluxes and thus air temperature. Temperature changes in the lower 1000 m of the NCV box are much larger in the dryCV case than in the dryCR or drySN cases; as such, only the dryCV case is shown (Figure 18). We briefly note that in the dryCR and drySN cases, temperature and pressure changes are much smaller (+/- 1 degree C and -0.4 hPa), and the pressure gradient strengthens in the late afternoon, largely corresponding to warming at boundary layer levels above the surface (150 m to 1200 m).

In the dryCV case, the NCV experiences strong low-level heating beginning in the morning, increasing in altitude as the boundary layer grows; temperature increases during day are well-mixed in the boundary layer. There is mild cooling over the OCN box at 200-330 m in the first week of the simulation. The strongest increase in temperature difference (warming of NCV relative to OCN) occurs late morning to late afternoon, at all levels below 690 m. At night, there is a small decrease in the low-level (<330 m) temperature difference. The corresponding strengthening of the pressure difference is also greatest from late morning to late afternoon. The mild strengthening of the pressure gradient on some nights (e.g.

early morning of June 28, June 29, July 3, July 9) appears related to longer nocturnal persistence of warming at NCV relative to OCN in the residual boundary layer (150 m - 690 m, although the elevation of warming differs among individual days).

3.2.3. Momentum budget timing and changes. The momentum advection, pressure gradient, and u time tendency terms in Equation 2 are estimated from model output (Figure 19). Using these three model-derived terms, we calculate the friction term as the residual (Figure 19, cyan line). The friction term has to vary diurnally in order to reproduce the observed wind diurnal cycle. The time tendency ($\frac{\partial u}{\partial t}$) term is much smaller than pressure gradient term, even in afternoon when the pressure gradient is largest and advection is small. If friction were not also large at this time, the wind would accelerate much faster. Conversely, high wind speeds persist even after the pressure gradient declines between 22:00 and 04:00, even with strong advection of lower momentum air. If friction during the night remained at its high afternoon values, the winds would decelerate at night. The decline in the friction term at night is necessary in order to explain the observed high winds at night. [cite LLJ paper of some sort - not the first time this is being said.] Moreover, this residual has the expected diurnal shape of friction, with high values in the daytime when convective turbulence creates a uniform boundary layer and high momentum flux to the ground, and low values at night when the residual upper boundary layer decouples from the shallow stable nocturnal boundary layer and is buffered from friction with the surface.

In the dryCV case, the pressure gradient term increases at all hours but especially between 10:00 and 18:00 (Figure 20), when it increases by 20% to 30% (cf. Figure 19). The advection term becomes more negative at those same hours, as

faster Solano wind transports lower momentum air more effectively. The friction term also becomes more negative in the daytime, probably due to greater instability and convection from the hotter Central Valley land surface. The changes in the dryCR and drySN cases were much smaller, with the pressure gradient term increasing by a maximum of 0.0001 to 0.0002 m/s² in the late afternoon.

3.2.4. Summary of mechanism. Solano wind responds to the near-surface pressure gradient between the Central Valley near the Solano pass and the central coast ocean. Changes in boundary layer temperature at either of these locations influences this driving pressure gradient. Soil moisture strongly influences land surface heating, and changes to soil moisture in the Central Valley strongly affect boundary layer temperature and thus near-surface pressure in the regions relevant to the Solano wind. When Central Valley soils are dry, the atmospheric boundary layer warms from late morning to late afternoon, strengthening the pressure gradient at those hours. At the same time, friction and advection of lower momentum air increase, due respectively to increased convection and faster lateral transport. These negative terms limit the increase of Solano winds to \sim 1.5 m/s on average in the late afternoon.

4. DISCUSSION AND CONCLUSIONS

Wind speed at the Solano Wind Project wind farm is sensitive to regional soil moisture, especially in the Central Valley. Drier Central Valley soil moisture increases Solano turbine-level wind by up to 3 m/s, and wetter Central Valley soil decreases Solano turbine-level wind by a similar amount. For a XX MW wind farm, an increase of 3 m/s from XX to XX (in the most sensitive range of the wind-power curve) would mean an increase of XX MW of generation. The changes are largest in the late morning to late afternoon, with average increases of \sim 1.5 m/s in the

late afternoon when Central Valley soil moisture is reduced from $0.25 \text{ m}^3/\text{m}^3$ to $0.1 \text{ m}^3/\text{m}^3$. Notably, these midday changes in wind speed coincide with the approximate timing of the daily wind ramp-up; thus, wind changes due to soil moisture errors are likely to shift the predicted timing of the ramp-up.

Understanding the mechanism behind the soil moisture effect lends credence to the reality of this influence in the real world, not just in the model, and helps to indicate other wind farm locations that might be similarly influenced by soil moisture. Soil moisture affects Solano wind by controlling land surface heating and thus influencing air temperature through the boundary layer. Changes in air temperature affect the near-surface pressure gradient that drives the Solano wind. Solano wind is most sensitive to pressure over the central coastal ocean and in the Central Valley. Soil moisture in the Central Valley influences Solano wind more strongly than soil moisture in the Coast Range or in the Sierra Nevada because the Central Valley soil moisture more directly controls the air temperature in the Central Valley regions relevant to the driving pressure gradient. The changes in pressure gradient and wind are concentrated in the late morning to late afternoon because the changes in land-surface heating and boundary layer air temperature are greatest at these times. Nevertheless, in the case of a dry Central Valley, the air temperature, pressure gradient, and wind speeds remain slightly elevated even at night. The marked increases in the pressure gradient are partially offset by negative changes in momentum advection (due to faster transport of lower-momentum air) and friction (due to increased convection), which limit the acceleration of the winds.

This study is a prototype, and several caveats and uncertainties bear mentioning. First, a more complete analysis should run the model for a longer time period

covering more synoptic, and ideally more seasonal, conditions. Also, running ensembles with perturbed forcing, to characterize uncertainty due to lateral forcing and model advection, would test the robustness of the results. The specific results are probably sensitive to PBL scheme and model resolution to some degree. However, the differences due to the PBL scheme would probably be a matter of degree rather than of the sign of the changes, since PBL schemes most directly affect vertical mixing and only indirectly affect lateral transport, which is most relevant to the horizontal pressure gradients controlling wind changes here. Additionally, we have followed guidelines from previous literature regarding PBL schemes and grid resolution that give good simulation accuracy [Marjanovic *et al.*, 2014; XX]. However, these model parameters and others would need to be chosen carefully to give best performance at a specific site [Wharton *et al.* YYYY].

There are also uncertainties related to the model representation of land surface heat and moisture fluxes. We expect the effect of letting soil moisture evolve over the day, rather than holding it fixed at every timestep, to be small, because the changes in soil moisture are small (Figure XX); moreover, allowing soil moisture to evolve dynamically is comparable to initializing a day-ahead forecast with erroneous soil moisture, in which case soil moisture would also evolve over the day. The results probably depend strongly on model land use and land cover, which determine albedo, plant transpiration dynamics, and roughness; the results would have been different if we had modified the land use distribution. Similarly, the results depend on the accuracy of the Noah LSM land cover and soil hydrology parameterizations; Chapter XX of this dissertation illustrates that the different stomatal dynamics of different plant species can change boundary layer air temperature, which this chapter shows is an important control on the pressure gradients driving near-surface winds.

Soil moisture in California varies both because of interannual variability in precipitation, causing anomalously wet or dry soils in the unmanaged mountain regions, and because of large-scale irrigation in the Central Valley. The area represented by the “CV” region in this study is certainly larger than the irrigated agricultural land area, and as such, the sensitivity of Solano winds to actual irrigation will be lower. However, these results show that correct estimation of soil moisture in both the agricultural and non-agricultural areas of the Central Valley is important for accurate Solano wind forecasts. More broadly, these results illustrate the sensitivity of winds in this NWP model, WRF, to soil moisture; because NWP models are widely used in wind energy forecasting, the accuracy of soil moisture input information is necessary for accurate energy resource forecasts, at least at sites like Solano. The effect of soil moisture is expected to be strongest when local and regional land surface heating drives winds, i.e. during the warm season with weak to moderate synoptic winds. In California, these conditions overlap with the season of greatest wind energy production, making soil moisture an important variable in wind energy forecasts. We also note that, while Solano winds are not strongly sensitive to Coast Range or Sierra Nevada soil moisture, other potential wind farm locations are strongly affected, including the northern and southern Central Valley (cf. Figure 7); future development of wind farms in these locations would benefit from measurements to constrain land surface energy fluxes in the Coast Range and Sierra Nevada.

Our hope is that studies of wind energy sensitivity to regional soil moisture can help constrain which measurements might improve wind energy forecasts. Soil moisture itself is difficult to measure at large scales and at the necessary depth [CITATION], and small-scale heterogeneity complicates the scaling-up of point measurements. As such, it may be more feasible and productive to measure a

related observable variable, such as land surface temperature (detected remotely from towers or aircraft using thermal imaging) or even the near-surface air pressure difference between the NCV region and the central coast, as proxies for soil moisture and the related land-surface heating. These measurements could be assimilated into NWP models using frameworks such as **CITE SOME LAND DATA ASSIMILATION PAPER**, or they could be integrated into statistical or machine-learning post-processing of NWP model output. We note that conducting model sensitivity studies such as this one could help constrain the regions to which the wind forecast is most sensitive and thus the regions with the greatest potential return on investment in measurement efforts.

Close with something here: refer back to motivation of wind variability and utility-scale integration. Better day-ahead to hour-ahead forecasts could reduce costs, and at many wind farm locations with a land-surface-heating component to driving the wind, improvements in soil moisture input information could help increase the accuracy of those forecasts. Help utilities manage the variability of wind energy cost-effectively and decrease the cost of wind energy.

5. REFERENCES

Electric Power Monthly with Data for July 2014

GE Energy, Western wind and solar integration study, May 2010.

IPCC

Jacobson, M. Z., and M. A. Delucchi

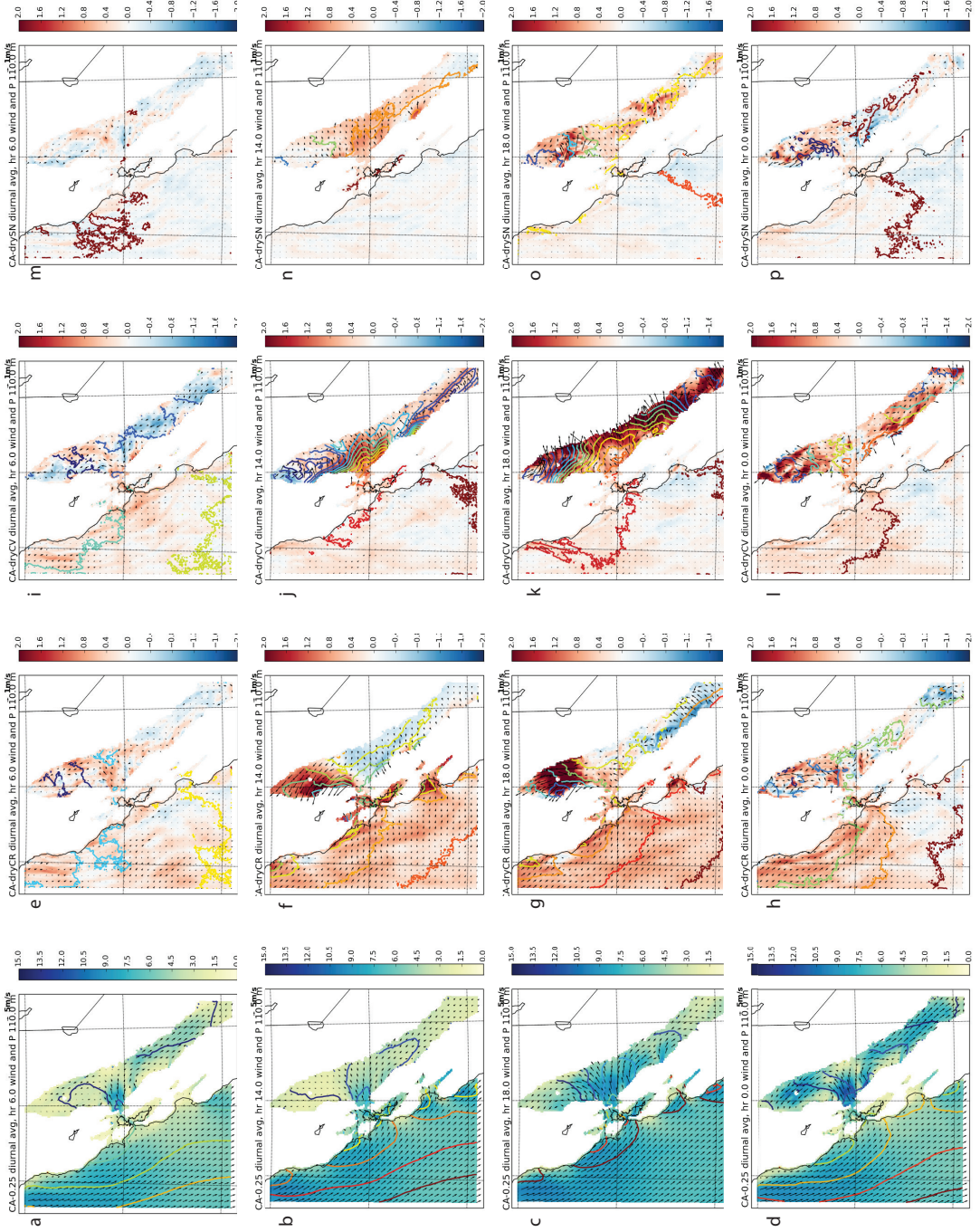


FIGURE 7. Wind speed (color shading) and direction (vectors) and pressure (color contours) at 110 m ASL on the d02 domain, averaged by hour over the two-week runs. (a)-(d) CA-0.25 control case. (e)-(h) dryCR case, changes in wind and pressure. (i)-(l) dryCV case, changes in wind and pressure. (m)-(p) drySN case, changes in wind and pressure. Top row: average for hour 06:00 for the whole run; second row: average for hour 14:00; third row: average for hour 18:00; bottom row: average for hour 00:00.

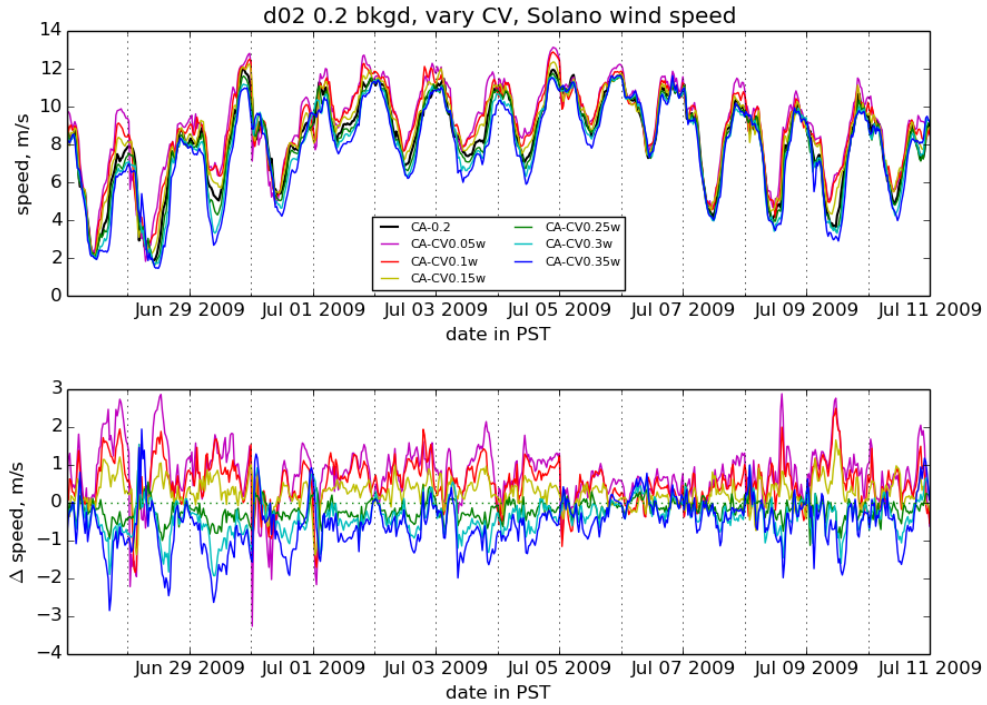


FIGURE 8. Time series of wind speed magnitude at 60 m AGL for the d02 grid point nearest the Solano wind farm, for a range of Central Valley soil moisture values, with soil moisture = 0.2 in the Coast Range and Sierra Nevada. (a) Wind speed time series, (b) time series of differences between test cases and control (CA-0.2). The model spin-up period is excluded.

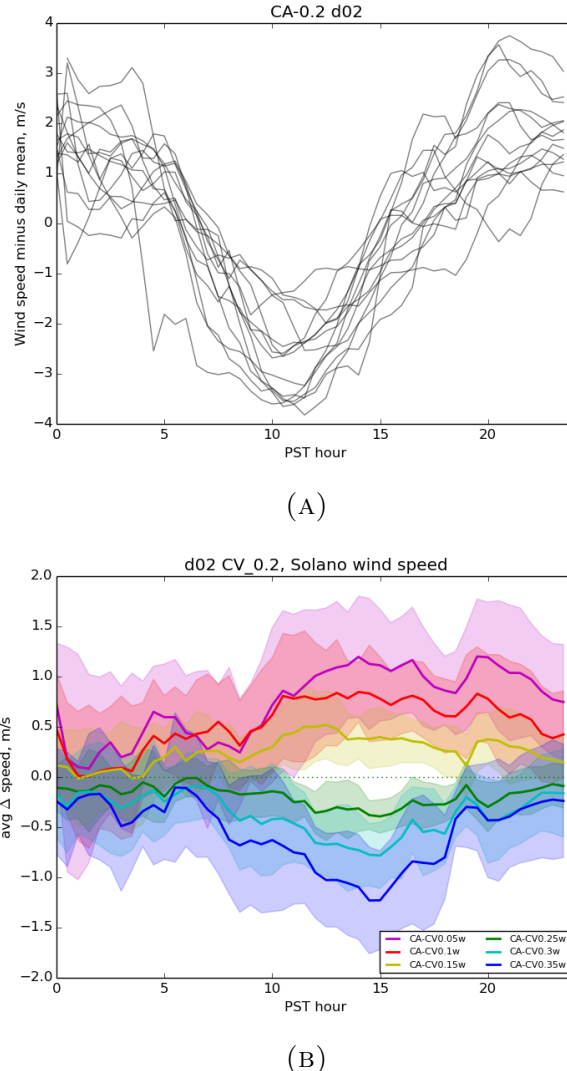


FIGURE 9. (a) Overlaid diurnal cycles of wind speed magnitude minus daily mean wind speed, at 60 m AGL for the d02 grid point nearest the Solano wind farm, for the CA-0.2 control case. (b) Diurnally averaged differences in wind speed, at 60 m AGL for the d02 grid point nearest the Solano wind farm, for a range of Central Valley soil moisture values. Shading represents one standard deviation.

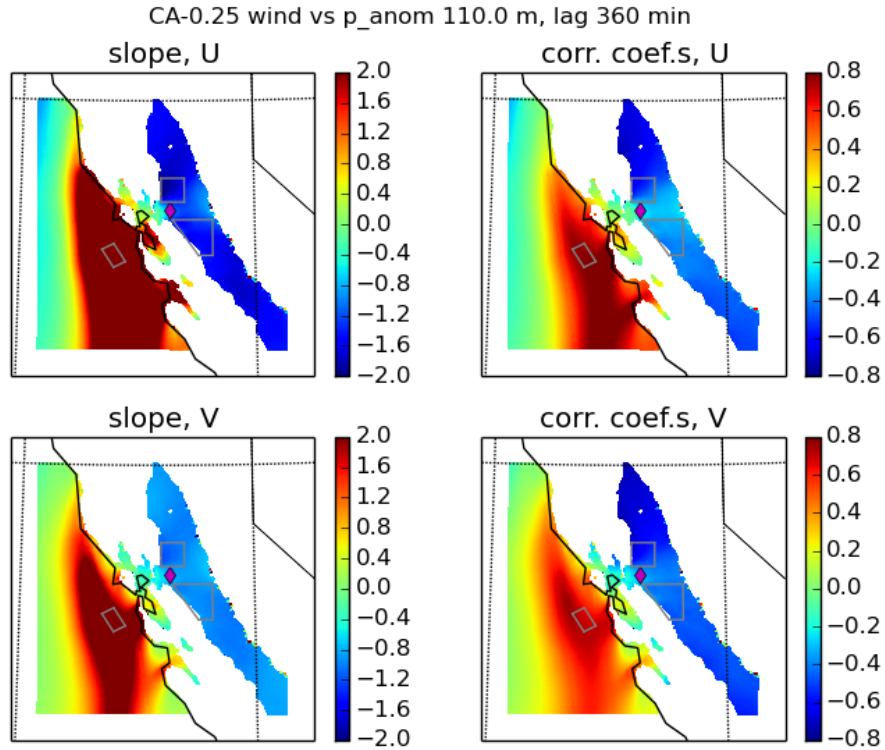


FIGURE 10. CA-0.25 case: Solano 60 m AGL (110 m ASL) wind linearly regressed against horizontal pressure anomaly at 110 m ASL, with wind lagging pressure by 6 hours. Top row: u -component of wind; bottom row: v -component of wind. Left column: linear regression slope; right column: correlation coefficient. Gray boxes outline areas used to calculate pressure gradients; ocean box is “OCN”, northern box in the Central valley is “NCV”, and southern box in Central Valley is “SCV”.

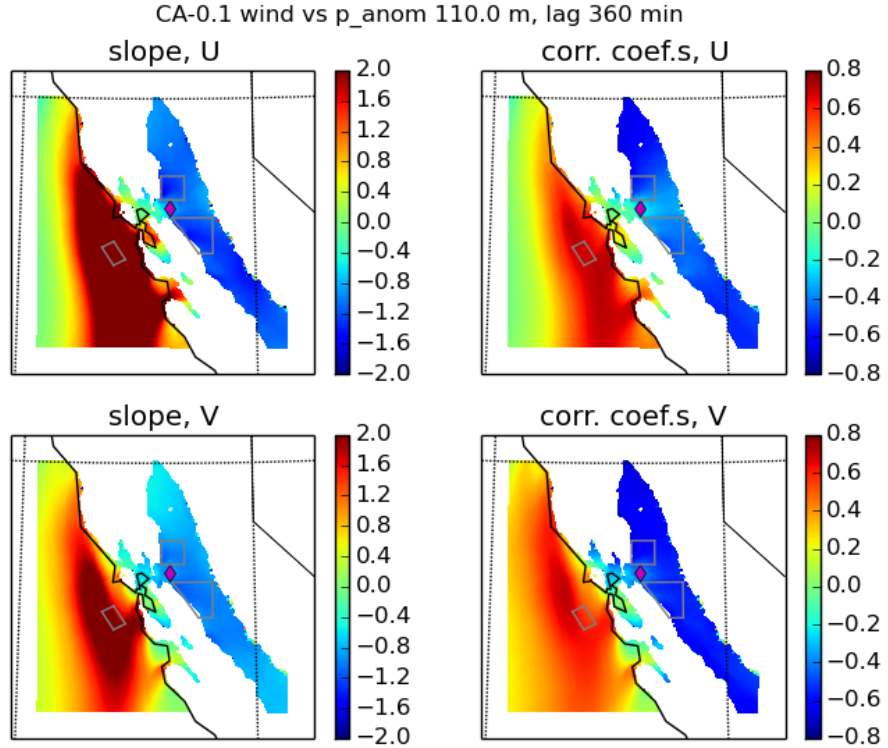


FIGURE 11. CA-0.1 case: Solano 60 m AGL (110 m ASL) wind linearly regressed against horizontal pressure anomaly at 110 m ASL, with wind lagging pressure by 6 hours. Top row: u -component of wind; bottom row: v -component of wind. Left column: linear regression slope; right column: correlation coefficient.

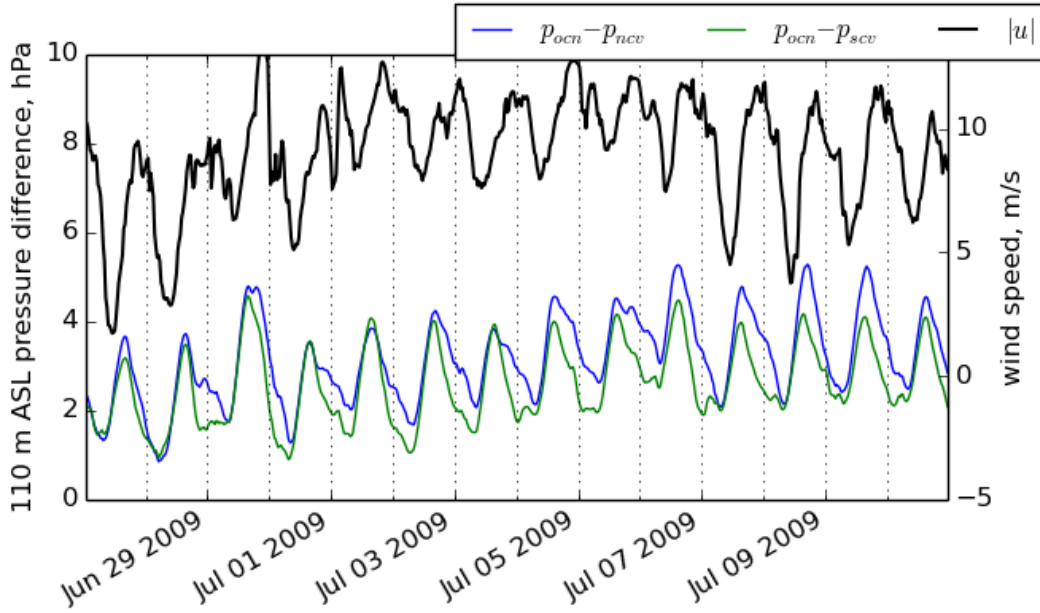


FIGURE 12. CA-0.1 control case: Solano 60 m AGL (110 m ASL) wind (black) and average pressure difference OCN box minus NCV box (blue) and OCN box minus SCV box (green) at 110 m ASL. The sign of the pressure difference is chosen to correspond with the $\frac{-1}{\rho} \frac{\partial p}{\partial x}$ term in the momentum budget.

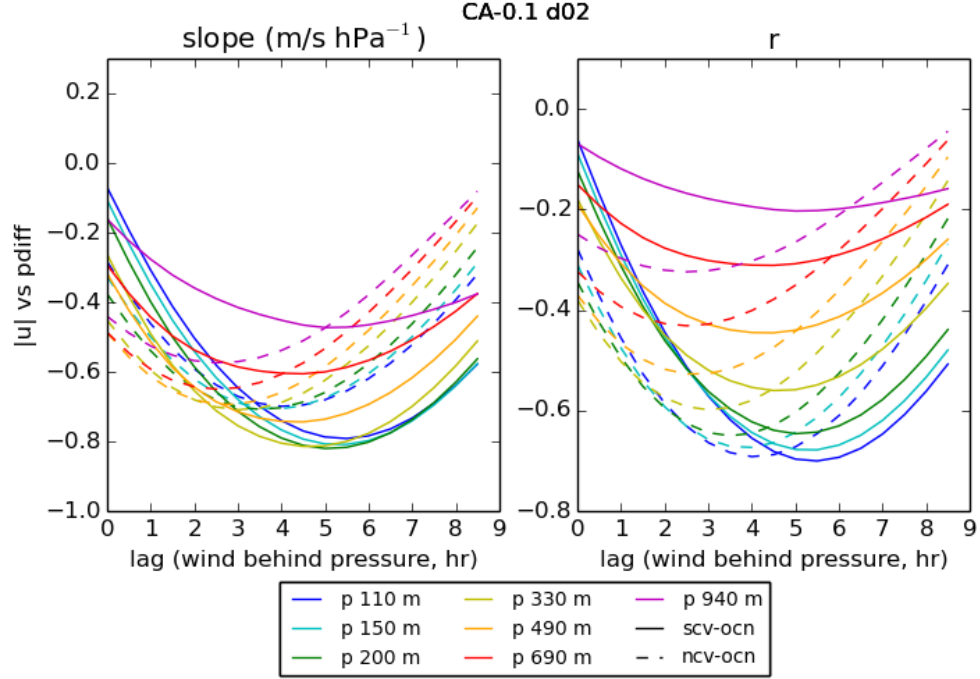


FIGURE 13. CA-0.1 control case: lagged linear regression of Solano 60 m AGL (110 m ASL) wind against average pressure difference NCV box minus OCN box (dashed) and SCV box minus OCN box (solid). Correlations are only shown for speed, because u and v velocity component results are very similar.

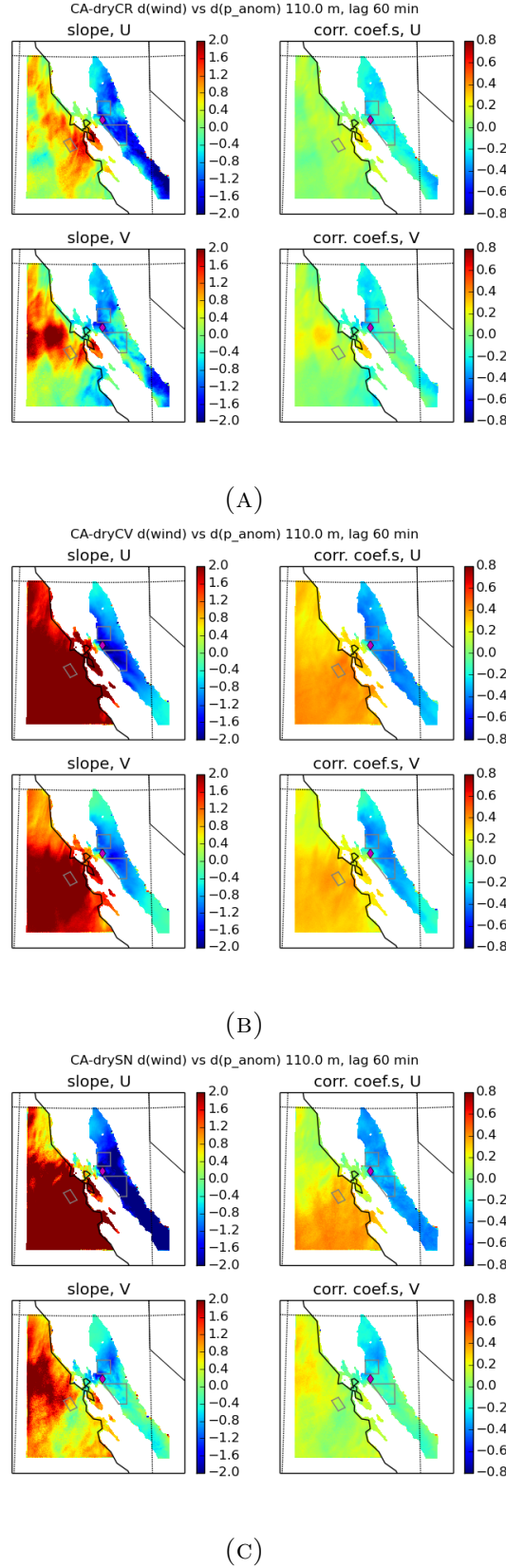


FIGURE 14. Correlation between Solano wind changes at 60 m AGL and horizontal pressure anomaly of change in 110 m ASL pressure, with a lag of 60 min, for the dry regional test cases minus control: (a) dryCR, (b) dryCV, (c) drySN. The order of panels is as in Figure 10.

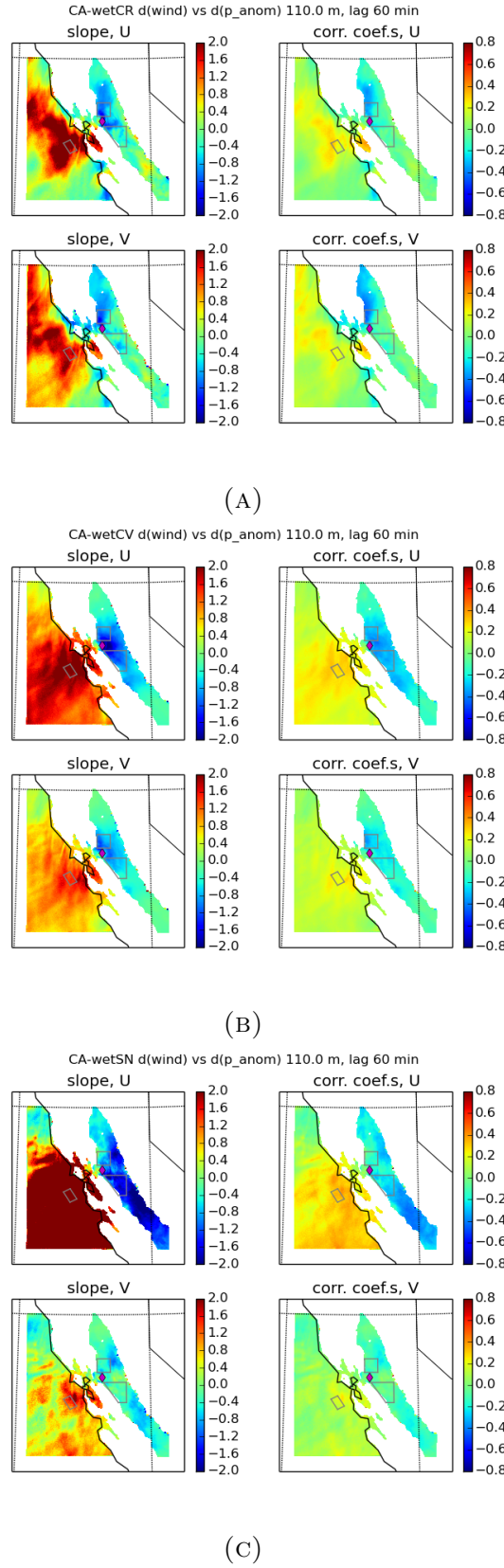


FIGURE 15. Correlation between Solano wind changes at 60 m AGL and horizontal pressure anomaly of change in 110 m ASL pressure, with a lag of 60 min, for the wet regional test cases minus control: (a) wetCR, (b) wetCV, (c) wetSN. The order of panels is as in Figure 10.

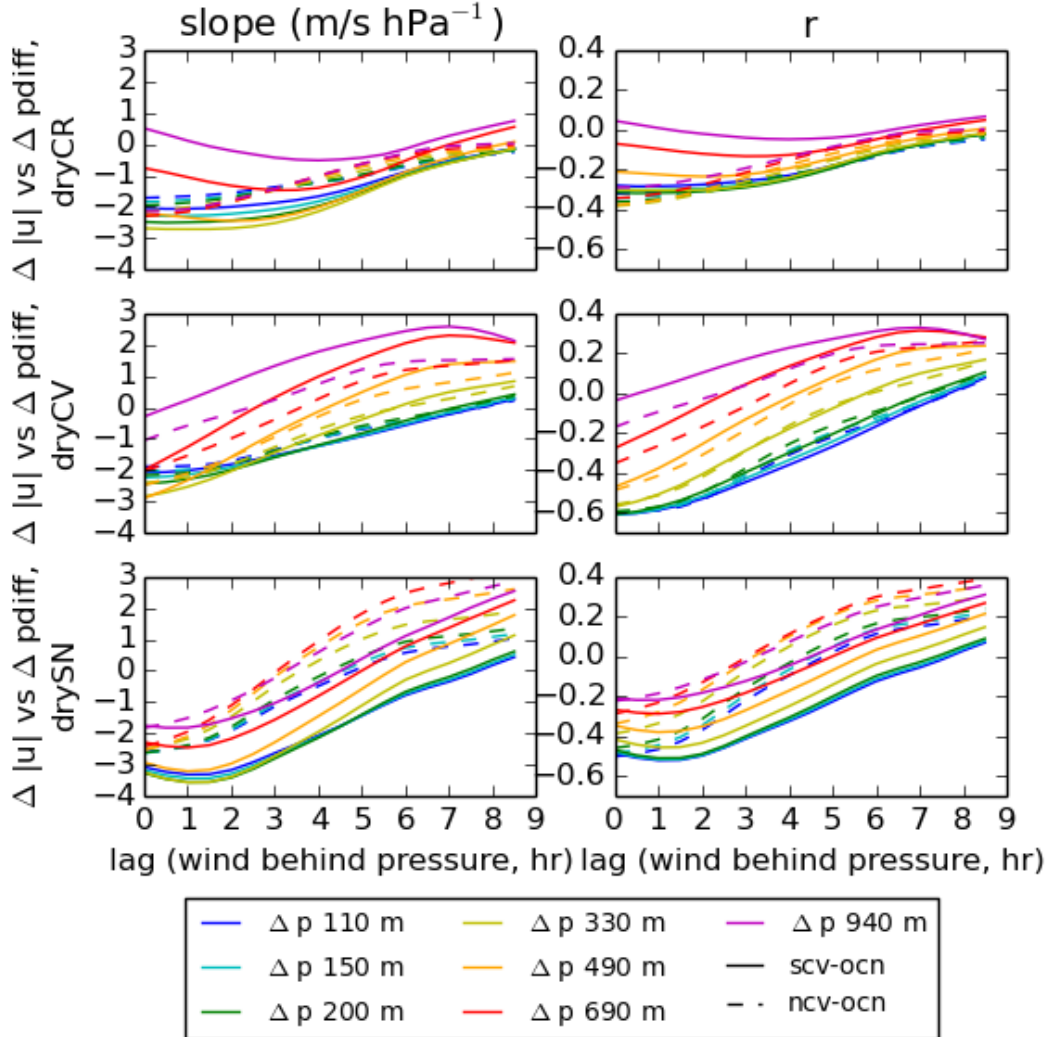


FIGURE 16. Dry regional perturbation cases: lagged linear regression of test-minus-control Solano 60 m AGL (110 m ASL) wind against test-minus-control average pressure difference NCV box minus OCN box (dashed) and SCV box minus OCN box (solid). Top row: dryCR; middle row: dryCV; bottom row: drySN.

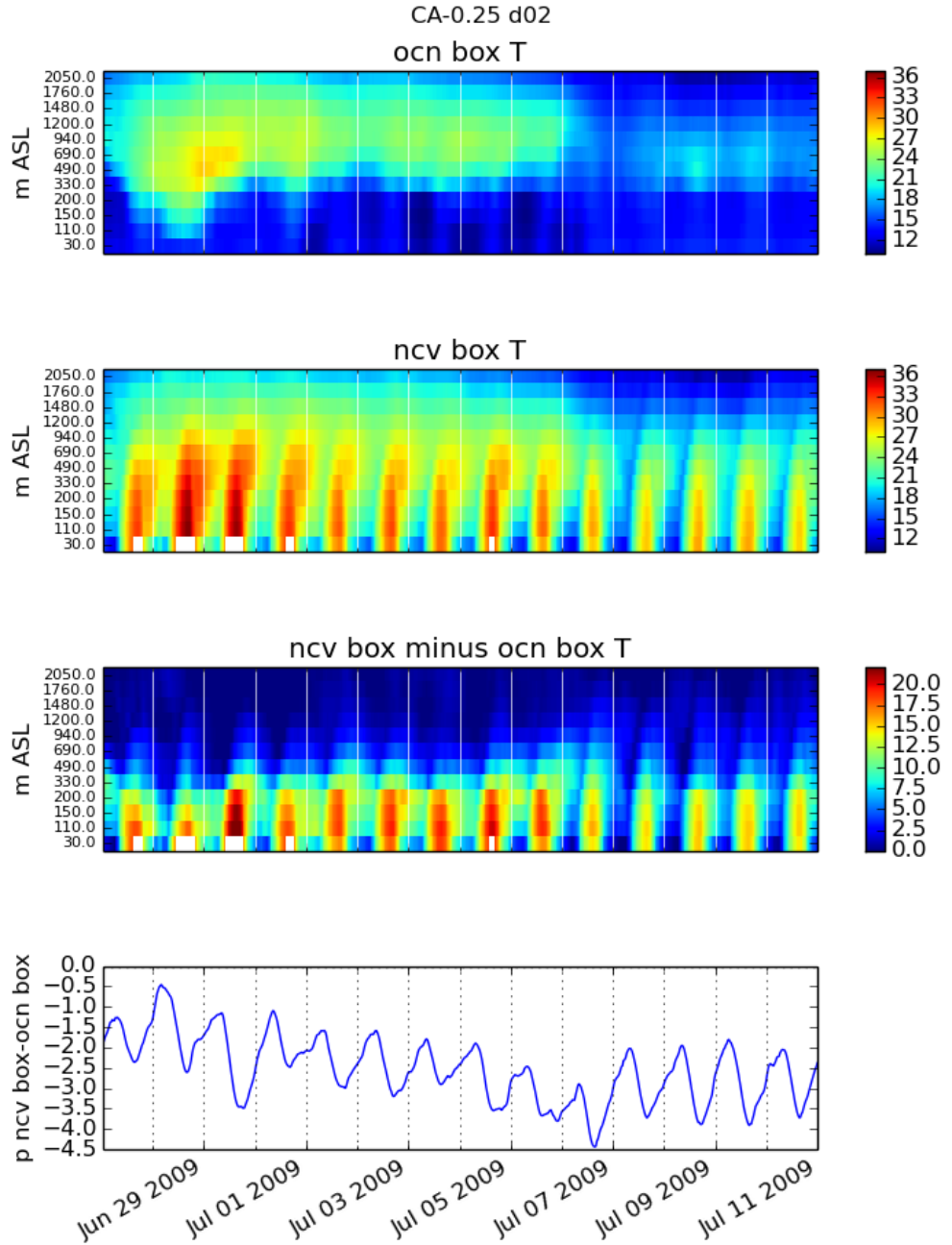


FIGURE 17. CA-0.25 control case: Temporal evolution of the vertical profile of temperature for the OCN box (top panel), the NCV box (second panel), NCV minus OCN (third panel); and time series of the NCV minus OCN pressure at 110 m ASL (bottom panel). White areas indicate times when the lowest σ model level was higher than 30 m ASL for the NCV box.

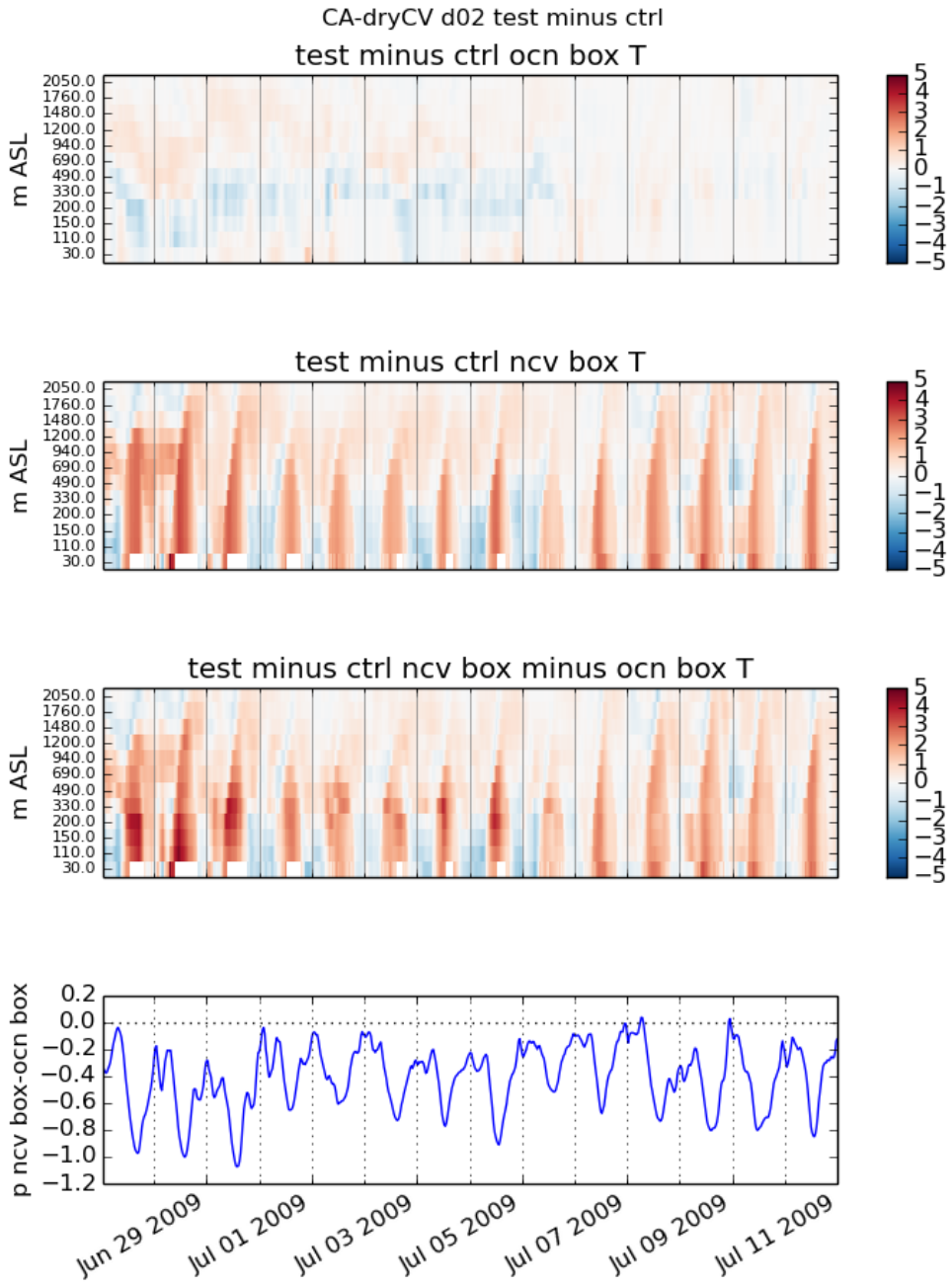


FIGURE 18. dryCV case: Temporal evolution of the vertical profile of test-minus-control temperature changes for the OCN box (top panel), the NCV box (second panel), NCV minus OCN (third panel); and time series of test-minus-control changes in the NCV minus OCN pressure at 110 m ASL (bottom panel). White areas indicate times when the lowest σ model level was higher than 30 m ASL for the NCV box.

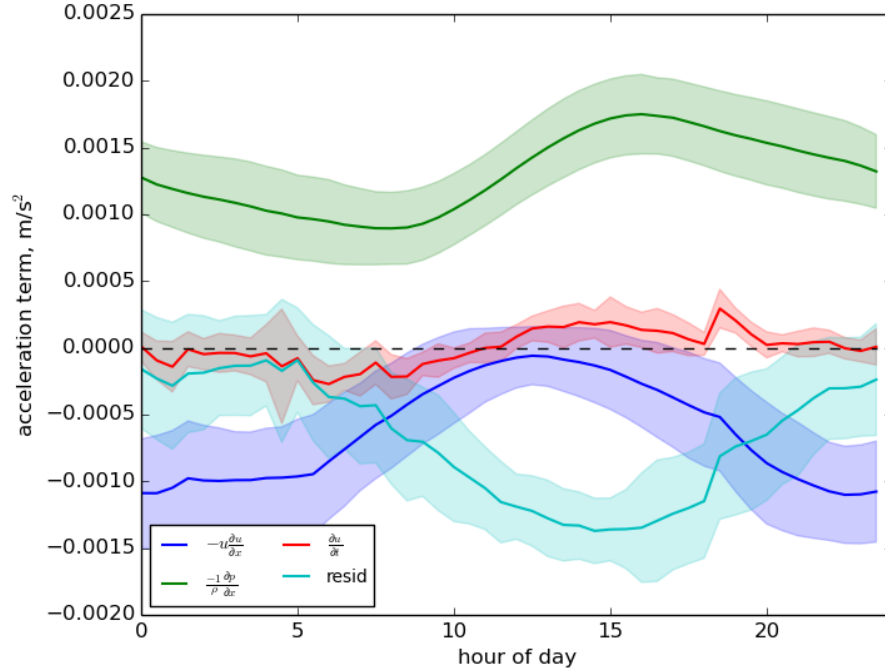


FIGURE 19. CA-0.25 control case: Diurnal average of terms of the momentum balance. Pressure gradient is calculated between the NCV and OCN boxes, and using density calculated at Solano 60 m AGL. Advection is calculated as $u_{solano} \frac{\partial u}{\partial x}$ with $\frac{\partial u}{\partial x}$ estimated with the gradient in wind between Solano and San Pablo Bay (the northern part of the San Francisco Bay). $\frac{\partial u}{\partial t}$ is calculated using Solano 60 m AGL wind speed. Friction (cyan) is calculated as the residual of the other three terms, following Equation 2. Shading represents one standard deviation.

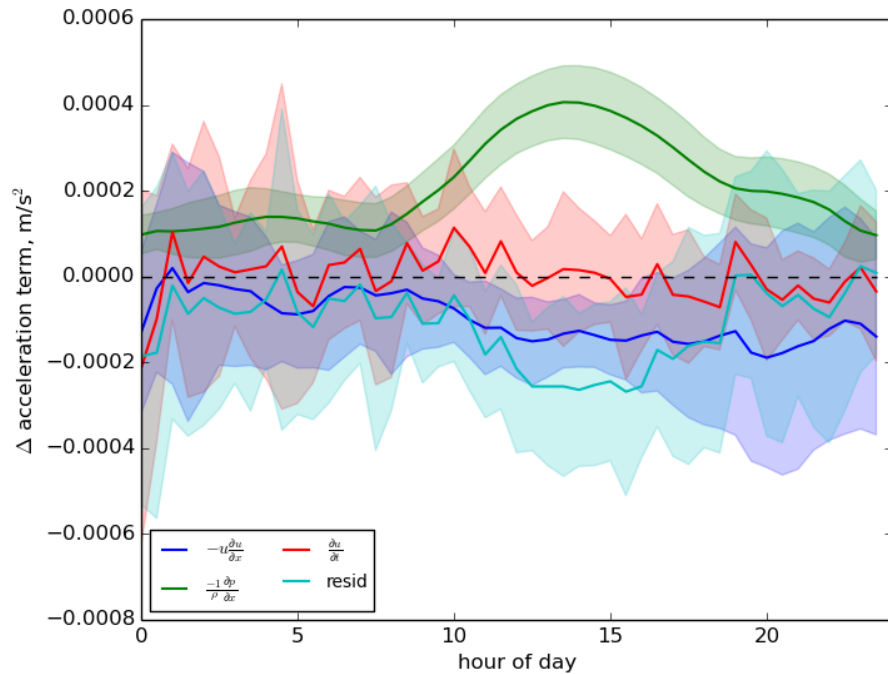


FIGURE 20. dryCV case: Diurnal average of test-minus-control change in terms of the momentum balance, calculated as in Figure 19. Shading represents one standard deviation.